Applied Catalysis B: Environmental 224 (2018) 660–670

Contents lists available at ScienceDirect

Applied Catalysis B: Environmental

journal homepage: www.elsevier.com/locate/apcatb

Research Paper

Desilicated NaY zeolites impregnated with magnesium as catalysts for glucose isomerisation into fructose

I. Graça[a,*], M.C. Bacariza[b], A. Fernandes[b], D. Chadwick[a]

[a] Department of Chemical Engineering, Imperial College London, Exhibition Road, London SW7 2AZ, UK
[b] Centro de Química Estrutural, Instituto Superior Técnico, Universidade de Lisboa, Av. Rovisco Pais, Lisboa 1049-001, Portugal

ARTICLE INFO

Keywords:
Glucose
Isomerisation
Fructose
Zeolites desilication
Magnesium

ABSTRACT

The impact of desilication on the performance of a series of alkali-treated NaY zeolites impregnated with 5 wt.% of magnesium for glucose isomerisation into fructose has been studied. Desilication at different NaOH concentrations increases the mesoporous volume and external surface area, without compromising microporosity and crystallinity. The observed reduction of the microporous volume due to magnesium impregnation was found to decrease for the alkali-treated zeolites. Higher density and strength of basic sites and stronger magnesium-support interaction were also achieved with the treatment. These improved properties resulted in a significant increase of both glucose conversion and fructose yield on the magnesium-doped desilicated zeolites. Glucose conversion continuously increases with desilication (28–51%), whereas fructose yield passes through a maximum (35%) at low desilication levels. Among the prepared desilicated samples, low-severity alkali-treated zeolites also show lower deactivation in consecutive reaction runs, as well as superior regeneration behaviour. Thus, hierarchical NaY zeolites impregnated with magnesium could be favourably used for glucose isomerisation into fructose if suitable alkaline treatment conditions are selected, with low-severity treated NaY zeolites being the best choice. Higher fructose productivities were achieved for the low-severity desilicated zeolites than for higher magnesium content NaY zeolites reported previously, leading to a lower Mg requirement.

1. Introduction

Increasing environmental concerns about the use of fossil fuels in the refining and petrochemical industry has turned worldwide efforts towards the development of processes based on renewable energy resources. Lignocellulosic biomass, a cheap, abundant and sustainable carbon source, has been a focus of attention from both industry and academia due to its great potential to be converted into fuels and value-added chemicals [1–4]. This has raised the interest in the study of saccharides transformations, mostly glucose, which is the main lignocellulosic biomass monomer [1,3,5–7]. A new range of applications for glucose have been investigated, such as its use as a raw-material for the production of fuels, important platform chemicals and polymers [1,3,8,9].

Glucose isomerisation into fructose is one of the key reactions in the biomass-derived glucose transformation chain for the production of chemicals and polymers, since fructose is an important starting material in the synthesis of numerous valuable bio-based compounds, such as levulinic acid, lactic acid or 5-hydroxymethylfurfural (HMF) [10–13]. The latter is a possible precursor for the production of caprolactam, the monomer for nylon-6 [14], while levulinic acid can serve as precursor for production of adipic acid [15].

Immobilised enzymes (D-glucose or xylose isomerase) have been traditionally applied as industrial catalysts for the isomerisation of glucose into fructose [16,17]. However, the search for a suitable chemical catalyst is essential for biomass valorisation, as it would make the process economically more attractive. Heterogeneous catalysts, in particular, present the advantages over homogeneous catalysts of being environmentally cleaner, more cost-effective and more easily regenerated and recycled. Basic solid materials were the first catalysts tested for glucose isomerisation into fructose, following the conventional Lobry de Bruyn–Alberda van Ekenstein mechanism [13]. Hydrotalcites, alkaline-exchanged and MgO-impregnated zeolites, anion-exchanged resins, mesoporous ordered molecular sieves of the M41S family, magnesium oxide and metallosilicate solid bases are among the already published materials [18–27]. The successful application of materials containing Lewis acid sites for the glucose isomerisation into fructose was more recently discovered, with Ti- and Sn-promoted zeolites and mesoporous silicas being the most studied solids [28–30].

Both basic and Lewis acid zeolites have been shown to be attractive

* Corresponding author.
E-mail address: i.graca@imperial.ac.uk (I. Graça).

https://doi.org/10.1016/j.apcatb.2017.11.009
Received 24 May 2017; Received in revised form 31 October 2017; Accepted 4 November 2017
Available online 06 November 2017

catalysts for glucose isomerisation into fructose at mild operating conditions. However, reduction of textural properties as a result of the addition of activity promoters has been one of the reported drawbacks. In fact, in our earlier work, the incorporation by impregnation of increasing amounts of magnesium oxide (up to 15 wt.%) to a NaY zeolite with the purpose of boosting the catalyst activity was observed to negatively affect fructose selectivity [27]. This was ascribed to a partial porosity blockage due to magnesium addition that increases fructose residence time inside the zeolite structure and so promotes its further transformation. References to limitations in the use of some zeolite structures due to their small pore size are commonly found in the literature, when using Ti- and Sn-containing zeolites [28–30]. It has been claimed that intermediate pore zeolites, such as the MFI, have only a residual activity when compared to BEA zeolites, as glucose molecules are too voluminous to diffuse along the narrow channels and access the active sites. However, if part of these active sites becomes accessible, activity can be greatly improved, as demonstrated by Li et al. [30] when studying Sn-zeolites by DFT. Sn-MWW and Sn-MFI are zeolites with similar pore size, but Sn-MWW is much more active than the Sn-MFI as intrazeolitic Sn sites are slightly more accessible in the MWW structure.

Diffusion inside zeolites can be significantly enhanced by generating mesoporosity into the structure through post-synthesis procedures. Desilication has been verified to be a very suitable method of obtaining combined micro- and mesoporous zeolites with preserved structural integrity [31]. This alkaline treatment allows a selective extraction of silicon from the framework such that framework aluminium is mostly maintained, the extent of Si and Al removal depending on the Si/Al ratio of the zeolite [31–33]. Moreover, mesoporosity is improved without greatly compromising the microporosity of the zeolite [34,35]. Therefore, these hierarchical zeolites have shorter micropore diffusion paths and enhanced access to micropores through the newly created mesopores [31], which can have a beneficial impact on the catalytic activity.

Hierarchical zeolites have not been extensively applied to glucose isomerisation into fructose, but the few existing studies have revealed a very positive influence of their use on both glucose conversion and fructose production [36–38]. The performances of a self-pillared, micro- and mesoporous Sn-MFI zeolite and a regular Sn-BEA zeolite were compared by Ren et al. [36]. For the same level of glucose conversion (85%), a much higher fructose yield was obtained with the hierarchical Sn-MFI zeolite (65 against around 35%). Alkali-treated Sn-MFI zeolites were also tested for the reaction [37]. No activity was found for the parent Sn-MFI zeolite, but glucose conversions between 13–21 and 35–41% could be achieved after 15 min and 2 h over the alkali-treated Sn-MFI zeolites. Fructose yields were also observed to gradually increase with the improvement of the mesoporous surface area. The effect of the desilication of a Sn-BEA was also simulated through DFT calculations [38]. It was noticed that the creation of additional silanol groups by the treatment can enhance the catalytic properties of the SnOH defect sites, as it increases the Lewis acidity of the active centres.

In the present work, hierarchical micro- and mesoporous NaY zeolites impregnated with 5 wt.% of magnesium have been investigated for glucose isomerisation into fructose for the first time. The purpose was to establish the effect of zeolite desilication on the catalytic performance for glucose isomerisation. Low to moderate-severity NaOH alkaline treatments were applied to the NaY zeolite, in order to achieve only a limited degree of desilication. By generating a controlled mesoporosity on the NaY zeolite, it was expected to overcome to some extent the loss of textural properties resulting from magnesium incorporation, improve molecular diffusion, and as consequence enhance glucose conversion and fructose yield. Characterisation of the alkali-treated NaY samples with or without magnesium has been performed by a combination of several techniques, including inductively coupled plasma optical emission spectroscopy (ICP-OES) for elemental analysis, X-Ray diffraction (XRD), N_2 adsorption, pyridine adsorption followed by Fourier transformed infrared (FTIR) spectroscopy, diffuse reflectance ultraviolet-visible (UV–vis) spectroscopy, solid state ^{27}Al and ^{29}Si magic-angle spinning (MAS) nuclear magnetic resonance (NMR), thermogravimetry and differential scanning calorimetry (TGA-DSC) and temperature programmed desorption of CO_2 (CO_2-TPD), in order to understand the impact of desilication on activity and selectivity. The effect of desilication on the deactivation trend and the possibility of regeneration of the catalysts are also studied. Overall, it is shown that low-severity desilicated NaY zeolites lead to improved activity and fructose productivity, and they are demonstrated to have the best regeneration capacity among the other desilicated zeolites.

2. Experimental

2.1. Catalyst preparation

The parent NaY zeolite was supplied by Zeolyst (CBV 100), with a global Si/Al ratio of about 2.73 given by elemental analysis. Alkali-treated samples were prepared through treatment of the parent NaY zeolite with aqueous sodium hydroxide (NaOH) solutions, at different concentrations (0.01-0.2 M) using a solution/zeolite ratio of 33 mL/g. After heating the NaOH solution up to 60 °C in a polyethylene bottle equipped with a reflux condenser, the parent sample was added and the mixture was kept at this temperature under stirring for 30 min. After the alkaline treatment, the zeolite suspension was immediately cooled down with an ice bath and filtered. The liquid filtrate was recovered and the extracted quantities of Si and Al were determined by inductively coupled plasma (ICP). Afterwards, the zeolite was washed with deionised water until neutral pH and dried overnight in the oven at 100 °C. In order to make sure that the alkali-treated zeolites were fully exchanged with Na, three consecutive ion-exchanges were carried out using a 2 M $NaNO_3$ aqueous solution at 25 °C for 4 h with a solution/zeolite ratio of 4 mL/g. After the ion-exchanges, samples were washed with deionised water, filtered, dried overnight in the oven at 100 °C and finally calcined at 500 °C under air flow. Na-exchanged alkali-treated zeolites were identified as $NaY_{concentration}$, where concentration refers to the NaOH solution concentration used for the treatment.

5 wt.% of magnesium was then incorporated on the parent and alkali-treated zeolites by incipient wetness impregnation, using magnesium nitrate hexahydrate ($Mg(NO_3)_2{\cdot}6H_2O$, Sigma-Aldrich, 99% purity) as precursor salt. An aqueous solution of the Mg salt with a water volume close to that of the zeolite pores was added drop-wise to the zeolite, while stirring. After that, samples were once again dried in an oven overnight at 100 °C and calcined at 500 °C under air flow. After magnesium impregnation, the parent zeolite was designated as 5% MgNaY and the alkali-treated samples as $5\%MgNaY_{concentration}$, where concentration refers to the NaOH solution concentration used for the treatment.

2.2. Catalyst characterisation

Si, Al, Na and Mg contents on the zeolites were determined by inductively coupled plasma optical emission spectroscopy (ICP-OES) using a Varian Vista MPX ICP-OES system.

XRD patterns were obtained in a PANalytical X'Pert Pro diffractometer, using Cu Kα radiation and operating at 40 kV and 40 mA. The scanning range was set from 5° to 80° (2θ), with a step size of 0.033° and step time of 20s. Crystallinity of the samples was calculated from the XRD data by dividing the integrated areas in the 15–35° range for each zeolite and an appropriate reference.

N_2 adsorption measurements were carried out at −196 °C on a Micrometrics 3Flex apparatus. Before adsorption, fresh zeolite samples were degassed under vacuum at 90 °C for 1 h and then at 350 °C overnight. Spent samples were degassed at 120 °C for 1 h. The total pore volume (V_{total}) was calculated from the adsorbed volume of

nitrogen for a relative pressure P/P_0 of 0.97, whereas the micropore volume (V_{micro}) and the external surface area (S_{ext}) were determined using the t-plot method. The mesopore volume (V_{meso}) was given by the difference $V_{total} - V_{micro}$. Average errors in the microporous and mesoporous volumes and external surface area are 0.005 and 0.007 cm^3/g and 2 m^2/g, respectively.

Zeolites acidity was measured by pyridine adsorption followed by IR spectroscopy on a Nicolet Nexus spectrometer. The samples were pressed into thin wafers (10–20 mg/cm^2). The wafers were pre-treated at 450 °C for 3 h under secondary vacuum (10^{-3} Pa). After this pre-treatment, IR spectra of zeolite samples were recorded. The samples were then cooled down to 150 °C and pyridine vapour was introduced in excess (200–300 Pa) in the IR cell at 150 °C and adsorbed onto the activated zeolite for 10 min. At the same temperature, the pyridine excess was removed for 30 min under secondary vacuum and the IR spectrum with pyridine was recorded.

DRS spectra in the UV–vis region were obtained in a Varian Cary 5000 UV–vis-NIR spectrophotometer, equipped with a Praying Mantis™ Diffuse Reflection Accessory, in the 200–800 nm range, using a spectral bandwith of 4 nm and a scan rate of 600 nm/s. Catalyst spectra were obtained using the Na-exchanged zeolites as references. The reflectance spectra were converted into the Schuster–Kubelka–Munk (SKM) function, F(R), and presented versus wavelength. The SKM function, F(R), was calculated from the reflectance at each wavelength using the expression: $F(R) = (1 - R)^2/2R$, where R is the ratio of the intensity of the light reflected by the sample to the one reflected by a standard.

Solid state ^{27}Al and ^{29}Si MAS NMR was carried out using a Varian VNMRS spectrometer. 1 M aluminium nitrate solution and neat tetramethylsilane were used as chemical shift references.

TGA-DSC analysis was performed on a Setsys Evolution TGA from Setaram instruments. Each sample (35–40 mg) was heated from 20 to 800 °C at 10 °C/min under air flow (30 mL/min). The weight loss and heat released were recorded as a function of the temperature.

Temperature programmed desorption (TPD) of CO_2 was carried out in a fixed-bed flow reactor. The sample (100 mg) was pre-treated in-situ at 450 °C by flowing 100 mL/min of N_2 for 1 h. After cooling to 50 °C, the sample was exposed to a 20% CO_2/N_2 mixture for 1 h. The system was then purged in flowing N_2 for 1 h to remove physisorbed CO_2, and the temperature was then increased to 800 °C at 10 °C/min. Desorbed CO_2 was analysed using a CO_x Siemens Ultramat 23 infrared detector.

Spent catalysts were analysed for the carbonaceous deposits after reaction using thermogravimetric analysis (TGA), which was carried out in a TA Instruments TGA Q500. The samples were heated up from room temperature to 800 °C, at 10 °C/min, under air flow (60 mL/min). The weight loss was recorded as a function of the temperature.

2.3. Catalytic test

Glucose isomerisation reaction was performed in a 25 mL Büchi AG autoclave at 100 °C under inert nitrogen atmosphere of 3 bar to avoid air entering the system. Before the reaction, a solution containing 0.5 g of D-glucose (Sigma, ≥99.5% purity) in 5 mL of deionised water was prepared and placed in the reactor, which already contained the catalyst (100 mg). The reactor was sealed, purged with nitrogen, and the initial working pressure was set. An oil bath was used to heat up the reactor, which was only introduced after the desired temperature was reached. The reaction was carried out for 2 h under continuous stirring (1000 rpm) to have a well-mixed condition and avoid external mass transfer limitations. After reaction, the reactor was cooled down, the nitrogen was released and the liquid product-catalyst suspension collected.

In order to analyse the liquid product the catalyst was firstly separated from the mixture by centrifugation at 5000 rpm for 5 min. All the liquid samples were diluted in water and analysed by high-performance liquid chromatography (HPLC) using a Shimadzu Prominence UFLC system equipped with a refractive index (RID-10A) detector. The analysis was carried out with a Supelcogel™ C-610H HPLC column, thermostated at 30 °C. The mobile phase was a 0.1% (v/v) H_3PO_4 aqueous solution at a flow rate of 0.3 mL/min. Citric acid was added as standard. The experimental errors in the conversion and yield are on average 2% and in the selectivity 7%.

Leaching of cations from the catalysts to the reaction mixture was analysed by inductively coupled plasma (ICP) using a Perkin-Elmer Optima 2000 DV ICP system.

Table 1
Si and Al extraction from the zeolite framework and Si/Al ratios for the Na-exchanged parent and desilicated zeolites.

Sample	Si_{ext} (mg/g)[a] (% Si_{ext})	Al_{ext} (mg/g)[a] (% Al_{ext})	Si/Al[b]	Si/Al[c]
NaY	–	–	2.73	–
$NaY_{0.01}$	0.6 (0.3)	0.04 (0.05)	2.65	2.73
$NaY_{0.02}$	0.8 (0.4)	0.07 (0.09)	2.80	2.73
$NaY_{0.05}$	1.8 (0.8)	0.3 (0.3)	2.60	2.72
$NaY_{0.1}$	2.4 (1.1)	0.4 (0.5)	2.68	2.72
$NaY_{0.2}$	4.0 (1.8)	0.6 (0.7)	2.52	2.71

[a] Determined from elemental analysis of the filtrate.
[b] Determined from elemental analysis of the solid sample.
[c] Determined from the filtrate elemental analysis and composition of the parent sample.

3. Results and discussion

3.1. Catalyst characterisation

3.1.1. Alkali-treated zeolite supports

The quantities of Si and Al found in the filtrate for the prepared NaY alkali-treated samples are presented in Table 1. As expected, low Si and Al extractions are obtained, as desilication of pristine faujasite zeolites using low to moderate alkaline treatment conditions is not usually as efficient as for ultra-stable Y zeolites (USY) [39,40]. However, the amounts of Si and Al removed from the zeolite gradually increase with the increase of the NaOH concentration. In addition, contrary to what observed for other zeolite structures with Si/Al ratio inferior to 20, for which Si removal is inhibited by the high aluminium content [32], there is still a selective removal of Si from the NaY. Due to the reduced Si and Al extractions, Si/Al ratios of the desilicated zeolites do not greatly differ from the Si/Al ratio of the parent zeolite, but a slight decrease of the ratio can be generally observed. Si/Al ratios obtained from elemental analysis and determined based on the Si/Al of the parent zeolite and the amounts of extracted Si and Al are observed to be in reasonable agreement.

Even though only small Si and Al removals were achieved, the alkaline treatments performed were able to enhance the NaY parent zeolite mesoporosity and external surface area by 25–103% and 8–20% respectively, which shows that the desilication was effective (upper part of Table 2). In general, both mesoporous volume and external surface area increase with the increase of the NaOH concentration, and so with the Si and Al removed from the zeolite (Fig. 1). On the other hand, the alkali-treatments did not lead to any significant changes in the microporous volume. Crystallinity for the desilicated zeolites was also not significantly affected by the treatment (Fig. 2, upper part of Table 2), with only a small decrease mainly seen for the most severely desilicated zeolites (treatment with 0.1 and 0.2 M NaOH).

Fig. 3 shows the 3800–3500 cm^{-1} OH-region of the FTIR spectra for the Na-exchanged parent and desilicated zeolites. No bands corresponding to the vibration of the bridging hydroxyl groups (Al—OH—Si) responsible for the Brønsted acidity of the zeolites were found in the spectra, as expected for fully Na-exchanged zeolites. The most visible band appears at 3745 cm^{-1} and is ascribed to the presence of non- or low-acidity terminal framework silanol groups (Si—OH) on the external surface [41,42]. The intensity of this band does not follow a clear

Table 2
Textural properties, crystallinity, amount of Lewis acid sites and basic sites and sodium and magnesium contents for all the samples.

Sample	V_{micro} (cm^3/g) (%variation)[a]	V_{meso} (cm^3/g)	S_{ext} (m^2/g)	Cryst. (%)	Lewis acid sites (μmol/g)[c]	Basic sites (μmol/g)[d]	Na content (%)	Mg content (%)
NaY	0.323	0.043	48	100	455	26	9.64	–
$NaY_{0.01}$	0.313	0.054	52	94	530	–	11.9	–
$NaY_{0.02}$	0.317	0.071	58	99	518	–	12.4	–
$NaY_{0.05}$	0.309	0.053	54	99	524	–	12.4	–
$NaY_{0.1}$	0.316	0.083	56	92	528	–	12.4	–
$NaY_{0.2}$	0.321	0.087	58	92	559	–	11.5	–
5%MgNaY	0.243 (25%)	0.045	49	92	360	101	7.26	5.02
5%$MgNaY_{0.01}$	0.262 (16%)	0.055	53	90[b]	–	98	9.71	5.04
5%$MgNaY_{0.02}$	0.261 (18%)	0.070	51	92[b]	–	190	9.26	5.16
5%$MgNaY_{0.05}$	0.249 (19%)	0.058	50	92[b]	429	185	9.84	5.00
5%$MgNaY_{0.1}$	0.247 (22%)	0.080	62	96[b]	–	154	9.03	5.13
5%$MgNaY_{0.2}$	0.241 (25%)	0.081	50	97[b]	378	154	8.43	4.68

[a] Variation of microporous volume due to magnesium addition.
[b] Calculated considering each Na-exchanged zeolite as 100%.
[c] Determined using the FTIR band at 1443 cm^{-1} after pyridine adsorption.
[d] Obtained from the CO_2-TPD profiles.

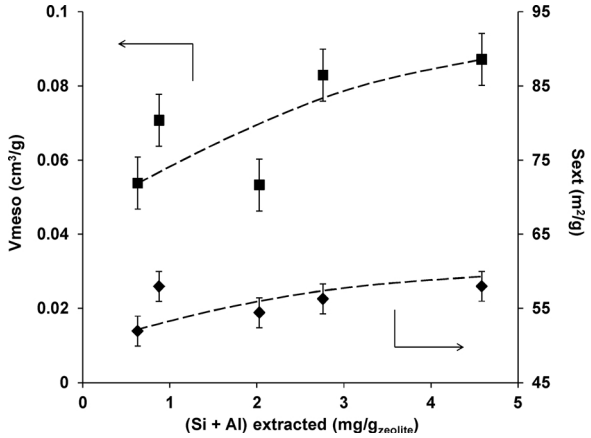

Fig. 1. Evolution of the mesoporous volume (■) and external surface area (♦) as a function of the total amount of Si and Al extracted from the zeolites. Dashed lines were included only to express the general tendency of the results.

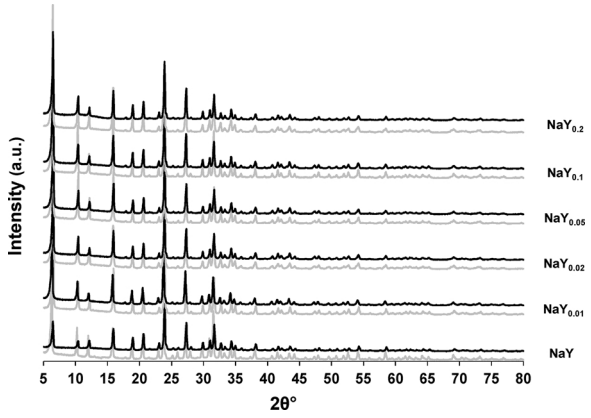

Fig. 2. XRD diffraction patterns for all Na-exchanged (grey lines) and 5 wt.% magnesium-impregnated zeolites (black lines).

evolution with the desilication degree, although it normally increases as a result of the creation of an additional mesoporosity on the outer surface of the zeolite crystal [43]. However, this comparison is not straightforward since the proton of some OH-groups in the silanol can also be replaced by Na [44]. The degree of this exchange might be higher for the desilicated zeolites as silanol groups should be more exposed due to the additional mesoporosity generated by the treatment.

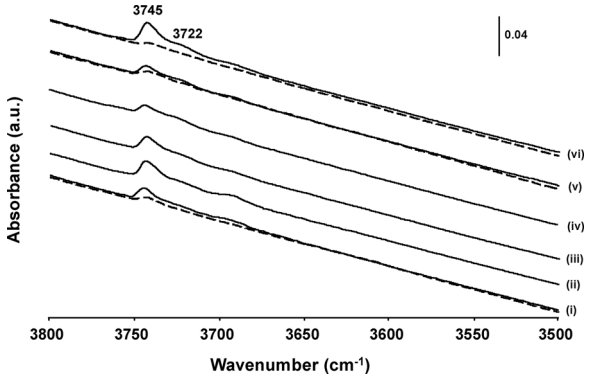

Fig. 3. 3800–3500 cm^{-1} region of the FTIR spectra for the (i) parent zeolites and desilicated zeolites at (ii) 0.01, (iii) 0.02, (iv) 0.05, (v) 0.1 and (vi) 0.2 M. Na-exchanged samples (black lines) and magnesium-impregnated samples (dashed lines).

Nevertheless, for the less ($NaY_{0.01}$) and the most ($NaY_{0.2}$) desilicated samples, it is possible to see that there is an enhancement of the number of external silanol groups when compared to the parent zeolite. A very small band at 3722 cm^{-1} can also be seen, but only for the desilicated samples. This is normally attributed to internal silanol groups corresponding to hydroxyl nests occurring at defect sites [41,45], and could be associated with the formation of an additional mesoporosity deeper inside the zeolite framework due to the alkaline treatment.

The presence of any type of acid sites on the zeolite samples was assessed by pyridine adsorption followed by IR spectroscopy. The difference spectra of the Na-exchanged parent and alkali-treated zeolites obtained by subtraction of the spectra after and before pyridine adsorption can be seen in Fig. 4a. In agreement with the absence of bands related to the bridging hydroxyl groups before pyridine adsorption, it is confirmed that none of the zeolites have Brønsted acid sites, as the spectra after pyridine adsorption do not present the IR band at 1545 cm^{-1} related to the pyridinium ions formed through pyridine interaction with this type of acid sites (PyH^+). Moreover, the typical IR band of the pyridine coordinated to extra-framework aluminium (EFAL) species at 1455 cm^{-1} is also not found in the spectra. Thus, despite some aluminium removal from the framework by the alkaline treatment (Table 1), the extracted aluminium does not seem to be retained inside the structure generating EFAL species. Instead, a very high intensity band appears at 1443 cm^{-1}, being characteristic of pyridine coordinated to Na^+ cations in compensating positions of the zeolite, considered as weak Lewis acid sites [46,47]. The presence of bands at 1598 and 1490 cm^{-1} also confirms this assignment, as well as the very small bands at 1628, 1616 and 1575 cm^{-1} [46,47]. The number of

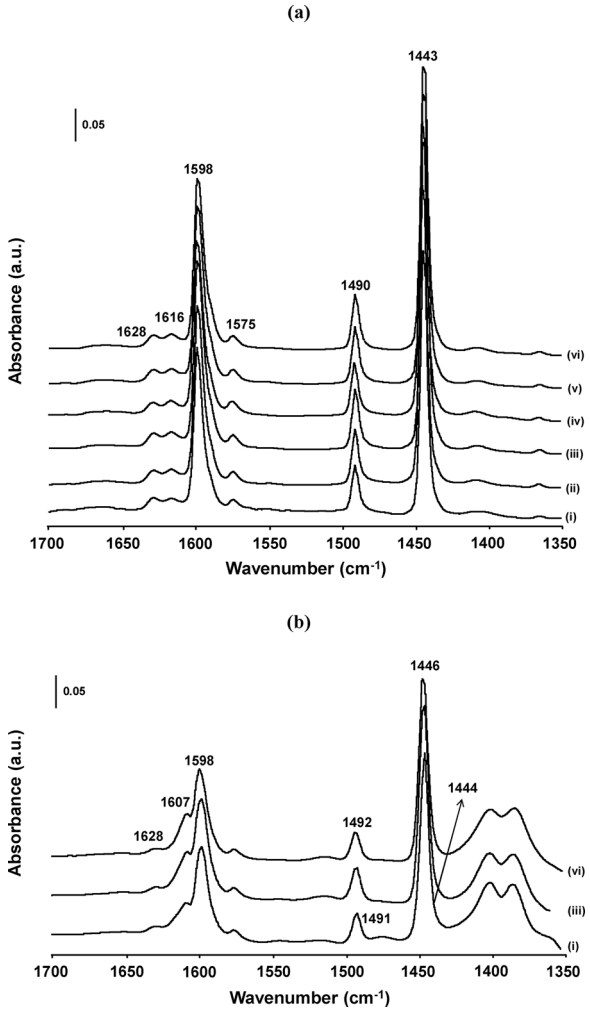

Fig. 4. Difference spectra after and before pyridine adsorption in the 1700–1350 cm^{-1} FTIR region for the (a) Na-exchanged and (b) magnesium-impregnated zeolites: (i) parent zeolite and desilicated zeolites at (ii) 0.01, (iii) 0.02, (iv) 0.05, (v) 0.1 and (vi) 0.2 M.

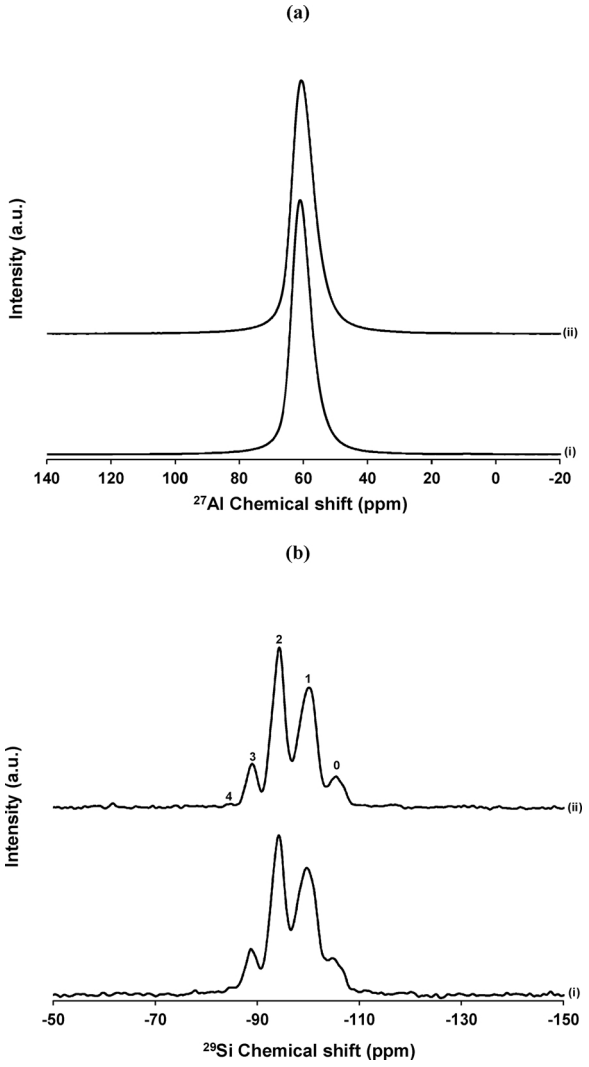

Fig. 5. (a) ^{27}Al and (b) ^{29}Si MAS NMR spectra for the Na-exchanged (i) parent zeolite and (ii) desilicated zeolite at 0.2 M.

these weak Lewis acid sites resulting from the presence of Na^+ was estimated for the different samples based on the area of the band at 1443 cm^{-1} and a previously determined extinction coefficient [48] (Table 2). Desilicated samples have a higher amount of these weak Lewis acid sites than the parent zeolite, as a consequence of their higher amount of sodium (Table 2). Sodium content increases for the alkali-treated zeolites due to the generation of new positions for Na-exchange, e.g. additional external and internal silanol groups.

In order to confirm the absence of extra-framework aluminium species and the possible existence of extra-framework silicon species derived from the alkaline treatment, solid state ^{27}Al and ^{29}Si MAS NMR were also performed on selected samples (Fig. 5). In agreement with the FTIR results after pyridine adsorption (Fig. 4a), no observable amount of EFAL species was detected in either the parent or $NaY_{0.2}$ desilicated zeolites, and only the typical signal of tetrahedrally coordinated framework aluminium at around 61 ppm was detected in the ^{27}Al MAS NMR spectra (Fig. 5a) [49,50]. Concerning the ^{29}Si MAS NMR spectra (Fig. 5b), they show the five signals of the typical Si(*n*Al) building units (n = 0–4) of the faujasite framework in the range −80 to −110 ppm. Only for the alkali-treated sample, another very low intensity peak can be seen at −117 ppm, which is probably indicative of the presence of a small amount of extra-framework silicon-rich species (EFSI) [49–51]. The retention of EFSI might be more important at higher desilication degree due to the greater Si extraction (Table 1).

3.1.2. Addition of magnesium

Powder XRD diffractograms obtained for the parent and desilicated samples containing magnesium (Fig. 2) show that zeolite structural integrity remains intact after the impregnation process. In fact, only a small decrease of intensity for the peaks related to the zeolite structure can be seen, leading to a very small apparent decrease of the crystallinity for the Mg-impregnated zeolites (lower part of Table 2). This is considered to be most likely related to the dilution effect resulting from the addition of 5 wt.% of magnesium in the final catalyst. No XRD phase associated with magnesium oxide was detected in the diffractograms (MgO: 2θ = 37.0, 43.0, 62.4, 74.8 and 78.7° [52,53]), as also previously reported [27], and so formed MgO entities might be amorphous or very small in size (< 3 nm).

Concerning textural properties (Table 2), a clear decrease of the microporous volume is noticed for the parent and alkali-treated zeolites with magnesium addition, whereas mesoporous volume and external surface area are not very much affected by the impregnation (a correction to the textural properties in reference [27] is included in the Supporting Information S.1). Results in Table 2 shows that in general for Y zeolites MgO particles prefer the interior of the structure where the microporosity is located, which could explain their apparent small size. Interestingly, the extent of the microporous reduction due to magnesium depends on the zeolite (Table 2), even if the samples have identical amount of Mg. A 25% reduction of the microporous volume

Table 3
Band gap energies for the fresh magnesium-impregnated zeolites and after consecutive reaction runs without and with regeneration.

Catalyst	Band gap energy (eV)		
	Fresh	After 3 runs	After 2 runs with regeneration
5%MgNaY	5.56	5.72	5.68
5%MgNaY$_{0.01}$	5.60	5.68	5.80
5%MgNaY$_{0.02}$	5.56	–	–
5%MgNaY$_{0.05}$	5.55	5.69	5.63
5%MgNaY$_{0.1}$	5.56	–	–
5%MgNaY$_{0.2}$	5.57	5.71	5.67

was estimated for the parent zeolite, but the negative impact of magnesium incorporation generally decreases for the desilicated samples as desilication might allow more space inside the structure to accommodate the magnesium oxide particles. However, this beneficial effect of desilication on the microporosity reduction due magnesium addition gradually decreases while increasing treatment severity. An explanation could be the increase of the MgO particles size due to the greater space available in the structure for samples with higher desilication degree. As MgO particles are not normally seen by XRD (Fig. 2) or TEM techniques [27], the relative size of the MgO entities in the samples was inferred by UV–vis spectroscopy by calculating the MgO band gap energies as these are normally proportional to the size of the particles [54,55]. It is important to note that DRS-UV–vis is a surface technique, meaning that mostly species on the outer surface of the zeolite and closer to the pore entrances are screened. Band gap energies were determined by plotting $F(R)^2$ as a function of the energy ($E = hc/\lambda$) and extrapolating the linear region to $F(R)^2 = 0$ [56–58]. Near identical values were obtaining for all the samples (Table 3), which suggests that the size of the MgO particles does not particularly change with the support. Nevertheless, retention inside the structure of extra-framework silicious species was observed to take place especially when high-severity alkaline treatments are applied (Fig. 5b), which could be responsible for the additional micropores blockage observed for these samples.

The analysis of the FTIR spectra before pyridine adsorption in the OH-region (Fig. 3) for the zeolites impregnated with magnesium indicates that MgO is interacting with both the external and internal silanol groups (Si—OH) [59,60], as shown by the reduction of the bands at 3745 and 3722 cm^{-1} when compared to the Na-exchanged zeolites. As the number of silanol groups is higher in the desilicated zeolites, as discussed in the previous section, magnesium should be interacting more with the alkali-treated zeolites than with the parent. Another interesting observation is the appearance of a new set of IR bands in the 1600–1200 cm^{-1} region that are not associated with the zeolite structure (Fig. 6). These bands seem to be related to the interaction between the samples and CO_2 molecules, even though a pre-treatment at 450 °C under secondary vacuum was performed before collecting the spectra. For all the catalysts, the most intense band appears at 1382 cm^{-1} and could be assigned to carbonate species formed in the vicinity of Mg^{2+} cations [61]. Another relatively intense IR band can be seen at 1396 cm^{-1}. This might be ascribed to the formation of unidentate carbonates for which desorption normally occurs at higher temperatures [62,63]. The presence of small amounts of bicarbonate species and bidentate carbonates can also be detected in the spectra at 1476 and 1352 cm^{-1} respectively [62,63]. These are usually less stable carbonate species and lower temperatures are required for their removal. In addition, a broad band can be found at 1272 cm^{-1}. The appearance of bands at 1270 cm^{-1} was previously reported for the adsorption of bidentate carbonate species on alumina and MgO [64–66]. This band is especially evident for the desilicated samples, showing the higher stability of the carbonate species when adsorbed on the alkali-treated zeolites. Hence, the presence of these bands on the Mg-

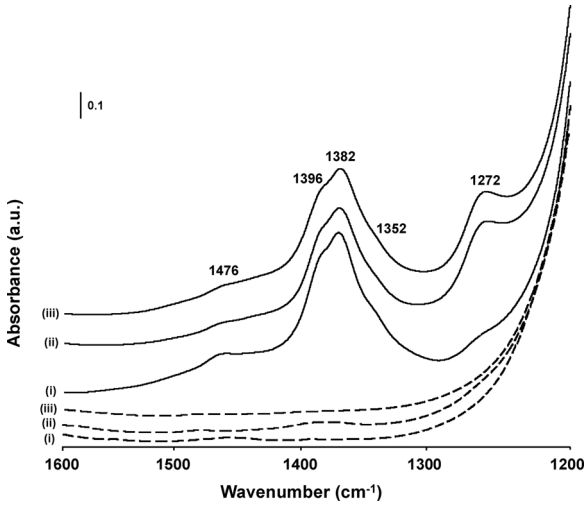

Fig. 6. 1600–1200 cm^{-1} region of the FTIR spectra for the magnesium-impregnated samples (black lines): (i) parent zeolite and desilicated zeolites at (ii) 0.05 and (iii) 0.2 M. Dashed lines – spectra of Na-exchanged zeolites for comparison.

impregnated zeolites already reveals an increase of the basicity relative to the samples containing only Na.

Concerning the IR spectra for the Mg-impregnated zeolites after interaction with pyridine (Fig. 4b), the same bands related to pyridine interaction with the Na^+ cations are detected. However, it is clear that there is a reduction of all these band intensities relative to the Na-exchanged zeolites (Fig. 4a). Consequently, a lower amount of Lewis acid sites was estimated for the Mg-impregnated zeolites (Table 2), which can be due to the smaller Na content found on the zeolites after magnesium addition (Table 2). The extent of the Na content reduction after Mg addition is not only a consequence of the lower relative amount of zeolite in these samples, but also shows that Na is removed during the impregnation process. This signifies that another cation should be compensating the zeolite framework, which could be H^+ due to the presence of some water or Mg^{2+} that remained as compensating cations instead of generating MgO. If protons were composing the framework, some Brønsted acid sites should have been detected after pyridine adsorption, which was not the case. Moreover, a slight displacement of the Na^+-pyridine bands at 1443 and 1490 cm^{-1} (Fig. 3a) to higher wavenumbers (1446 and 1492 cm^{-1}, Fig. 3b) can be noticed. This could be associated with the replacement of a small number of sodium atoms by magnesium, since if pyridine is coordinated to Mg^{2+} instead of Na^+ a shift of the main band from 1442 to 1449 cm^{-1} normally occurs [67]. The appearance of a new band at about 1607 cm^{-1} could also prove that Mg^{2+} is present in the framework, as bands 1608–1605 cm^{-1} have been assigned to pyridine coordination to divalent cations [68]. The displacement of the 1443 cm^{-1} band appears to be slightly higher for the Mg-impregnated desilicated zeolites, as well as the intensity of the 1607 cm^{-1} band is much stronger than for the parent zeolite, indicating that more Na^+ are replaced by Mg^{2+} in the alkali-treated samples. This could possibly already suggest that the strength of the interaction between magnesium and the desilicated zeolites is enhanced relative to the parent zeolite.

In order to confirm desorption of species at high temperatures in the samples containing magnesium, TGA-DSC analysis was carried out (Fig. 7). Data show two different endothermic weight losses, one from 50 to 350 °C that might be mostly related to the desorption of water from the zeolites and another starting at temperatures higher than 450 °C. This could be associated with the removal of adsorbed atmospheric CO_2, confirming the presence of CO_2 molecules very strongly interacting with the Mg-impregnated zeolites, as observed in the FTIR measurements (Fig. 6) noted above. Interestingly, it can be seen that CO_2 desorption begins at slightly higher temperatures for the

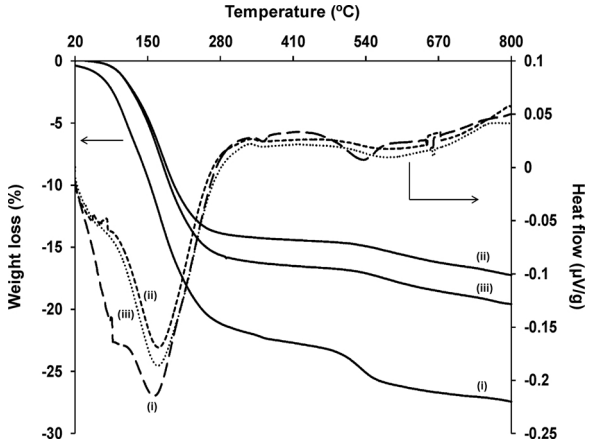

Fig. 7. TGA-DSC profiles for the magnesium-impregnated (i) parent zeolite and desilicated zeolites at (ii) 0.05 and (iii) 0.2 M.

desilicated samples than for the parent zeolite. Furthermore, for the alkali-treated zeolites, the second mass loss appears to be more gradual with the increase of the temperature, whereas it is rather abrupt for the parent zeolite in the beginning of the desorption process. Both phenomena could be already an indication that basic sites on the desilicated zeolites are stronger than on the parent zeolite, as they seem to be capable of retaining the CO_2 molecules up to higher temperatures.

The analysis of the number and strength of the basic sites on the Mg-impregnated zeolites was accomplished by CO_2-TPD measurements (Fig. 8). The Mg-impregnated NaY zeolite shows a main broad CO_2 desorption peak between 100 and 350 °C, which corresponds to the interaction of CO_2 with weaker basic sites. These can be the surface hydroxyl groups of the MgO that lead to the formation of bicarbonate species when in contact with CO_2 molecules and some weaker $Mg^{2+}-O^{2-}$ pair sites generating bidentate carbonates [69–71]. Thus, the first mass loss observed in the TGA-DSC experiments (Fig. 7) was not only due to water evaporation, but it might also have a contribution from CO_2 desorption. In addition, for this sample, a very small desorption peak can be seen at 550–800 °C, revealing that some stronger basic sites are also present, in agreement with the second weight loss in the TGA-DSC experiments (Fig. 7). This could be related to the desorption of stronger bidentate carbonates and/or monodentate carbonates formed on isolated surface O^{2-} ions (low-coordination anions) present in the defects of the MgO surface [69–71]. Concerning the magnesium-promoted desilicated zeolites, generally the same CO_2 desorption are found in the TPD profiles. However, it can be noticed that the area of the CO_2 desorption band at higher temperature is much more significant than for the parent zeolite. Furthermore, it can also be seen that there is a gradual shift of the low temperature desorption peak to higher temperatures with the degree of desilication. These results clearly demonstrate the increased basicity strength of the Mg-impregnated desilicated zeolites, which seems also to increase with the severity of the treatment. This confirms the higher stability of the carbonate species adsorbed on the alkali-treated zeolites, as observed by TGA-DSC (Fig. 7) and infrared spectroscopy. In addition to the strength, density of basic sites (estimated as the capacity to adsorb CO_2) is also higher in the Mg-impregnated desilicated zeolites than for the parent zeolite (Table 2), which is consistent with the greater amount of Na in the desilicated samples (Table 2), since the quantity of magnesium is the same as for the parent zeolite.

Thus, it was shown that the Mg-impregnated desilicated zeolites have improved characteristics relative to the parent zeolite in that they have enhanced textural properties, basicity and stronger magnesium-support interaction.

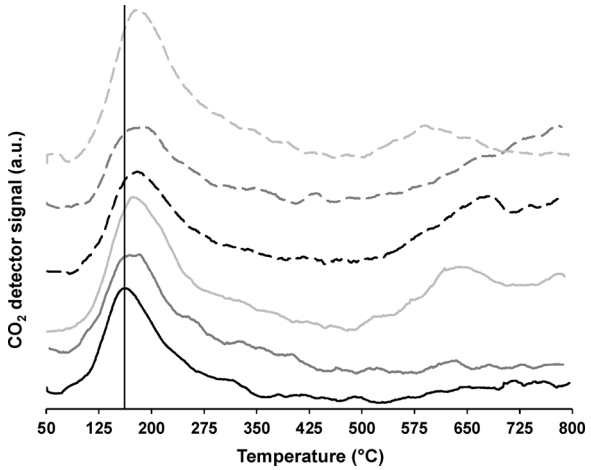

Fig. 8. CO_2-TPD results for the magnesium-impregnated zeolites: 5%MgNaY (black line), 5%$MgNaY_{0.01}$ (dark grey line), 5%$MgNaY_{0.02}$ (light grey line), 5%$MgNaY_{0.05}$ (dashed black line), 5%$MgNaY_{0.1}$ (dashed dark grey line) and 5%$MgNaY_{0.2}$ (dashed light grey line).

3.2. Catalytic performance

Desilication affects several properties of the catalysts as has been reported above, which can be expected to have a significant impact on their catalytic performance. Indeed, both glucose conversion and fructose yield (and selectivity) can be simultaneously affected by the porosity and basicity (density and strength of basic sites) changes introduced by the alkaline-treatment, so that the overall performance of the Mg-impregnated desilicated zeolites is dependent on a combination of several factors, as discussed further below. The relative contribution of the homogeneous and heterogeneous catalysis for the reaction is also analysed in this section. Finally, a comparison between the performances of the 5 wt.% Mg desilicated zeolites and higher Mg content NaY zeolites is presented.

3.2.1. Glucose conversion

Glucose conversion, fructose yield and selectivity obtained for the parent and desilicated zeolites impregnated with magnesium are presented in Fig. 9. Contrary to what has been observed by other authors on hydrotalcites, magnesium oxide and Sn-containing catalysts [13,25,28], mannose was not detected in any significant amount in the liquid product for the Mg-impregnated zeolite catalysts (Supporting Information S.2). Very low glucose conversions were reached for the Na-forms of the zeolites (3.4-6.6%, see Supporting Information S.3), and no changes were noticed with the desilication. In fact, these conversions are shown below to be associated with Na leaching. On the

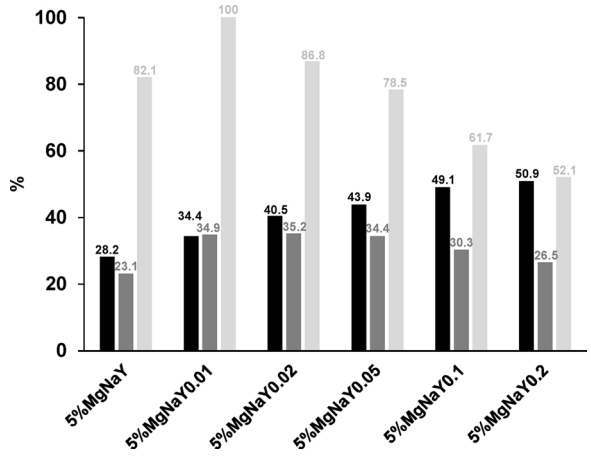

Fig. 9. Glucose conversion (black), fructose yield (grey) and fructose selectivity (light grey) for the parent and desilicated magnesium-impregnated zeolites, at 100 °C after 2 h.

other hand, a significant improvement of the activity of the catalysts with the level of the desilication is seen after magnesium addition. Glucose conversion increases by 22–81% relative to the parent zeolite over the samples desilicated at increasing NaOH concentrations (0.01-0.2 M). The observed beneficial effect of the desilication on the conversion could be due to the enhanced diffusion of the bulky glucose molecules within the zeolite porous system and the improved accessibility to the basic sites, as a result of the additional increase of the mesoporous volume generated by the alkali-treatment (Table 2). Indeed, the higher the mesoporous volume of the desilicated samples, the higher the conversion improvement. Besides this, the fact that the number of basic sites (Table 2) of the Mg-impregnated desilicated samples is in general higher than that of the parent zeolite, and that the basicity strength slightly increases with the severity of the treatment (Fig. 8), would also contribute to the observed increase of the conversion. Basicity cannot only promote the direct glucose isomerisation into fructose, but also the further glucose or fructose transformation. Therefore, the higher conversions obtained for the highly desilicated zeolites could also derive from the occurrence of glucose or fructose secondary transformations catalysed by these samples, which is consistent with their much lower fructose selectivities. In addition, it is important to remark that the relative increase of the glucose conversion with the level of desilication when compared to the parent zeolite seems to be higher for the samples treated at lower NaOH concentrations (0.01 and 0.02 M), progressively decreasing when using 0.05–0.2 M (Fig. 9). Three reasons can be suggested for this behaviour: (i) greater blockage of the microporous volume observed after magnesium addition for the more severely desilicated zeolites (Table 2) that can negatively influence glucose diffusion and access to the basic sites, (ii) the approach to the thermodynamic glucose conversion (57% at 100 °C [72]) and (iii) a higher level of deactivation for the more desilicated if more coke is seen on these samples due to the higher space available to accommodate coke molecules, as discussed below.

3.2.2. Homogeneous contribution

In our earlier papers [27,73], Mg-impregnated NaY zeolites were shown to suffer a degree of Na and Mg leaching in aqueous medium (a correction to the Na and Mg leaching results in reference [27] for the pre-leaching test is given here in the Supporting Information S.4). For the present desilicated zeolites, the homogeneous contribution for the reaction was analysed in a similar way [27]. Firstly, the catalysts were exposed to water at 100 °C for 2 h, under nitrogen and stirring. The catalysts were afterwards removed by centrifugation, and glucose was added to the collected liquids and reacted using the same operating conditions. Na and Mg extracted during water pre-leaching step and resulting homogeneous conversions can be seen in Table 4. For all Na-exchanged zeolites, observed activity appears to be 100% due to the leached Na. In the case of the Mg-impregnated samples, homogenous glucose conversion increases from 9% for the parent zeolite to a maximum of 15–16% for the desilicated samples. This shows that the homogenous contribution to the reaction is still limited for the alkali-treated zeolites impregnated with magnesium, even though both the quantities of Na and Mg leached from the desilicated samples are actually higher. Despite this, among the desilicated zeolites, magnesium removal appears to generally decrease with the severity of the treatment, perhaps because of the observed strengthening of the interaction between Mg and the support, as shown by CO_2-TPD and by infrared spectroscopy (see above). Nevertheless, as for the parent zeolite, the homogeneous contribution for the desilicated samples accounts for about 30–40% of the total conversion. Even though the homogeneous reaction is significant, the main contribution to the reaction appears to come from the heterogeneous catalysis, which is affected by modifications in the structure and properties of the samples introduced by the alkaline treatment. This contrasts with what was observed previously for other zeolite structures [73]. Higher Na and Mg leaching is observed during a normal reaction run in presence of glucose, see below section 3.3, which may impact on the contribution from the homogeneous reaction.

Table 4
Sodium and magnesium leaching from the catalysts after contact with liquid water at 100 °C for 2 h and homogeneous glucose conversions.

Catalyst	Na leaching ppm[a] (%)[b]	Mg leaching ppm[a] (%)[b]	Homogeneous glucose conversion (%)
NaY	36 (1.9)	–	6.8
$NaY_{0.01}$	36 (1.5)	–	4.1
$NaY_{0.02}$	34 (1.4)	–	6.8
$NaY_{0.05}$	62 (2.5)	–	4.1
$NaY_{0.1}$	33 (1.3)	–	4.8
$NaY_{0.2}$	39 (1.7)	–	4.5
5%MgNaY	113 (7.8)	2.0 (0.2)	9.1
5%$MgNaY_{0.01}$	160 (8.2)	11 (1.0)	11.2
5%$MgNaY_{0.02}$	216 (11.7)	5.9 (0.6)	15.7
5%$MgNaY_{0.05}$	210 (10.7)	5.3 (0.5)	15.0
5%$MgNaY_{0.1}$	181 (10.0)	6.5 (0.6)	15.5
5%$MgNaY_{0.2}$	158 (9.4)	4.5 (0.5)	15.2

[a] Concentration of Na or Mg in the liquid product (5 mL) after reaction.
[b] Percentage of Na and Mg removed considering their amount on each sample.

3.2.3. Fructose yield and selectivity

Fructose yields are also observed to be higher for all Mg-doped desilicated zeolites than for the parent sample (Fig. 9), as a result of the higher activity of these samples. However, contrary to the glucose conversion that always increases with the extent of the alkaline treatment performed, fructose yield (and selectivity) passes through a maximum when using 0.01–0.02 M NaOH solutions. This is a consequence of the increasing basicity strength with the severity of the alkaline treatment (Fig. 8), as highly basic materials were observed previously to lead to the formation of a higher amount of by-products [13,27]. In addition, the fact that the microporous volume, where the basic sites are located, tends to decrease slightly with the increase of the NaOH treatment solution concentration for the Mg-impregnated zeolites (Table 2) can also contribute to a promotion of fructose further conversion, as residence time of fructose molecules inside the zeolite structure might be higher. Hence, the highest fructose selectivities (100–87%) were achieved for the zeolites desilicated at 0.01–0.02 M due to the lower extent of secondary fructose transformations on these samples. Some by-products were detected in the liquid product by HPLC when the selectivity was not 100%. Attempts have been made to try to identify these by-products, but this identification has not been possible with the available analytical techniques, and further investigation is required. Nevertheless, it has been shown previously that it is possible to match the initial amount of carbon in the reaction mixture and the quantity of carbon in the liquid product after reaction through analysis of the total organic carbon (TOC) [27].

3.2.4. Influence of desilication vs. higher Mg contents

If one compares the catalytic performances of the desilicated zeolites after impregnation with 5 wt.% of magnesium (Fig. 9) and the parent zeolite (NaY) containing higher Mg contents (10 and 15 wt.%) reported previously [27], it can be seen that at the same operating conditions higher fructose yields are obtained for the desilicated zeolites treated with 0.01–0.05 M NaOH solutions (34–35%) than for high magnesium content NaY zeolites (32%), with a lower amount of glucose being also consumed. This means that desilication of the NaY zeolite is preferable to overloading it with magnesium, not only because less magnesium is required, but also in terms of green chemistry metrics, since less waste is produced per glucose molecule converted.

3.3. Deactivation and regeneration

During glucose isomerisation into fructose in presence of water over

Table 5
Sodium and magnesium leaching and coke retention on the magnesium-impregnated parent and desilicated zeolites, after 2 h of reaction at 100 °C.

Catalyst	Na leaching ppm[a] (%)[b]	Mg leaching ppm[a] (%)[b]	Coke (wt.%)
5%MgNaY	527 (36.3)	75 (7.5)	3.6
5%MgNaY$_{0.01}$	765 (41.3)	106 (10.5)	2.8
5%MgNaY$_{0.02}$	630 (34.0)	118 (11.4)	2.3
5%MgNaY$_{0.05}$	616 (31.3)	127 (12.7)	3.6
5%MgNaY$_{0.1}$	460 (25.5)	228 (22.2)	5.4
5%MgNaY$_{0.2}$	623 (37.0)	219 (23.4)	3.6

[a] Concentration of Na or Mg in the liquid product (5 mL) after reaction.
[b] Percentage of Na and Mg removed considering their amount on each sample.

Mg-impregnated NaY zeolites, Na and Mg leaching and coke accumulation appear to be the main mechanisms leading to deactivation [27]. In a normal reaction cycle, both Na and Mg extractions are observed to be higher than in a pre-leaching test (Table 5), as a result of the glucose and/or fructose contribution to the leaching due their chelating properties [27,74], meaning that the homogeneous contribution could potentially be more pronounced as the reaction proceeds. Mg leaching with the degree of desilication appears to be always more important than Na removal. Hydroxylation of the MgO surface due contact with water is claimed to be the first step during glucose isomerisation over bulk MgO, leading to the glucose C-2 deprotonation [25]. However, MgO hydration leads to its dissociation, and so to the release of Mg^{2+} to the water [75]. In addition, contrary to what was found in the pre-leaching test, magnesium content in the reaction medium increases with the degree of desilication when glucose is present from the beginning. This could be due to the higher exposure of the interior of the structure to glucose molecules for higher desilication degrees. The greater Na leaching found for the alkali-treated zeolites could be only a consequence of the higher Na content in these samples after desilication treatment (Table 2). On the other hand, coke content on the desilicated samples remains practically the same as for the parent zeolite (Table 5), meaning that the higher volume available might help the bulkier molecules to exit the zeolite structure more easily. This shows that deactivation due to coke deposition is not higher for the more severely desilicated zeolites, as previously speculated.

The study of the deactivation of the zeolites in repeated reaction cycles and their ability to be regenerated were also studied. Consecutive reaction runs were carried out always at the same operating conditions (100 °C, 2 h of reaction). Three cycles were performed with the catalyst being only washed with deionised water between steps, and in a separate study two reaction runs were carried out with intermediate regeneration by calcination under air at 600 °C for 1 h. Deactivation and regeneration were investigated for three representative desilicated samples: 5%MgNaY$_{0.01}$, 5%MgNaY$_{0.05}$ and 5%MgNaY$_{0.2}$. The results are given in Tables 6 and 7, where it is compared to the results previously obtained for the 5%MgNaY zeolite [27]. In agreement with the results for the parent zeolite, if no regeneration is done, a decrease of the glucose conversion with the number of runs can be seen for all desilicated zeolites. This is not only a result of the Na and Mg leaching (Table 6), but also of some degree of metal oxide particles agglomeration, which is revealed by the increase of the band gap energies relative to the fresh samples (Table 3). Some decrease of the crystallinity of the zeolites after the reaction cycles can also be observed (Table 8). Furthermore, it can be seen that the activity loss seems to increase slightly with the degree of desilication. This could be a consequence of the progressive increase of the Na and Mg leaching, since neither the MgO particles size (similar band gap energies, Table 3) nor the crystallinity (Table 8) on the desilicated zeolites after 3 reaction runs are significantly changed when compared to the parent zeolite.

Nevertheless, upon oxidative treatment at high temperature, the samples can almost fully or partially recover their initial activity (Tables 6 and 7). This clearly supports the previously reported benefit

Table 6
Glucose conversion and fructose selectivity, as well as Na and Mg leaching, for the magnesium-impregnated parent and desilicated zeolites, after consecutive runs at 100 °C after 2 h, without regeneration of the catalyst.

Catalyst	Run	Glucose conversion (%)	Fructose selectivity (%)	Na leaching ppm[a] (cumul. %)[b]	Mg leaching ppm[a] (cumul. %)[b]
5%MgNaY	1	28.2	82.1	539 (37.1)	72 (7.2)
	2	17.3	88.2	102 (44.1)	12 (8.4)
	3	11.5	97.3	62 (48.4)	14 (9.8)
5%MgNaY$_{0.01}$	1	38.5	92.2	626 (32.2)	139 (13.8)
	2	16.3	99.2	139 (39.4)	10 (14.7)
	3	13.9	97.3	77 (43.3)	7 (15.4)
5%MgNaY$_{0.05}$	1	42.3	76.5	614 (31.2)	153 (15.3)
	2	16.3	95.8	101 (36.4)	6 (15.8)
	3	15.2	86.3	70 (39.9)	6 (16.4)
5%MgNaY$_{0.2}$	1	52.2	52.2	650 (38.6)	164 (17.5)
	2	18.9	93.9	152 (47.6)	8 (18.4)
	3	15.8	90.4	92 (53.0)	13 (19.8)

[a] Concentration of Na or Mg in the liquid product (5 mL) after reaction.
[b] Cumulative percentage of Na and Mg removed considering their initial amount on each sample.

Table 7
Glucose conversion and fructose selectivity, as well as Na and Mg leaching, for the magnesium-impregnated parent and desilicated zeolites, after consecutive runs at 100 °C after 2 h, with regeneration of the catalyst.

Catalyst	Run	Glucose conversion (%)	Fructose selectivity (%)	Na leaching ppm[a] (cumul. %)[b]	Mg leaching ppm[a] (cumul. %)[b]
5%MgNaY	1	28.3	85.5	543 (37.4)	78 (7.8)
	2	26.9	93.1	154 (48.0)	72 (14.9)
5%MgNaY$_{0.01}$	1	36.6	96.5	601 (31.0)	141 (14.0)
	2	32.4	94.7	296 (46.2)	158 (29.7)
5%MgNaY$_{0.05}$	1	41.6	78.7	612 (31.1)	151 (15.1)
	2	35.1	82.2	306 (46.7)	151 (30.2)
5%MgNaY$_{0.2}$	1	51.2	52.6	564 (33.5)	165 (17.7)
	2	29.2	98.1	300 (51.3)	173 (36.2)

[a] Concentration of Na or Mg in the liquid product (5 mL) after reaction.
[b] Cumulative percentage of Na and Mg removed considering their initial amount on each sample.

of a regeneration step between reaction runs [27], which comes from a combination of the coke removal and redistribution of the magnesium oxide onto the supports. The latter can be confirmed by the slightly smaller size of the MgO particles after regeneration than without, despite the very high temperature applied (Table 3), as well as by the increase of leaching in the second run (Table 7). However, it is important to note that the capacity of the samples to have their activity restored decreases significantly with the level of desilication, maybe as a consequence of the higher magnesium leaching.

On the other hand, as also previously reported for the 5%MgNaY zeolite [27], fructose selectivity for the alkali-treated zeolites increases in consecutive reaction runs, both without and with regeneration (Tables 6 and 7). This becomes especially evident with the increase of the desilication degree as selectivities were initially much lower. The reduction of the basicity due to the Na and Mg leaching associated with the considerable improvement of the textural properties (Table 7) observed after the reaction cycles, as well as coke combustion in the case of the regenerated samples, can explain this more limited further transformation of fructose.

Table 8
Carbon accumulation, textural properties and crystallinity after consecutive runs without and with regeneration.

Catalyst	Run	Coke (wt.%)	V_{micro} (cm^3/g)	V_{meso} (cm^3/g)	S_{ext} (m^2/g)	Cryst.[b] (%)
5%MgNaY	After 3	2.7	0.266	0.159	80	82
	After 2 with intermediate regeneration[a]	2.3	0.251	0.158	93	75
$5\%MgNaY_{0.01}$	After 3	2.1	0.221	0.218	122	69
	After 2 with intermediate regeneration[a]	2.7	0.194	0.194	99	76
$5\%MgNaY_{0.05}$	After 3	3.3	0.234	0.209	108	79
	After 2 with intermediate regeneration[a]	2.3	0.242	0.245	118	76
$5\%MgNaY_{0.2}$	After 3	4.5	0.215	0.241	137	76
	After 2 with intermediate regeneration[a]	4.3	0.193	0.204	125	81

[a] Spent sample with coke.
[b] Crystallinity calculated considering each Na-exchanged zeolite as 100%.

4. Conclusion

Desilication of the parent NaY zeolite at different NaOH concentrations resulted in an increase of both the mesoporous volume and external surface area, while preserving the microporous volume and crystallinity. Addition of magnesium leads only to some decrease of the micropores, this effect being reduced by the desilication. Magnesium-doped alkali-treated zeolites also revealed higher density and strength of basic sites, as well as stronger magnesium-support interaction.

Both glucose conversion and fructose yield were remarkably increased over Mg-impregnated desilicated zeolites when compared to the parent zeolite. Enhanced performance was a result of the improved textural and basic properties, as activity was observed to be mainly governed by heterogeneous catalysis. Glucose conversion gradually increases with the degree of desilication (28–51%), while a maximum fructose yield of 35% is achieved when using low concentration NaOH solutions. High fructose selectivities > 87% are obtained for the low-severity desilicated zeolites.

Deactivation in consecutive reaction steps without regeneration increased with the desilication degree, as a result of the higher Na and Mg leaching for these samples. Nevertheless, upon high temperature treatment under air, desilicated zeolites can still recover part of their initial activity, especially for lower desilication level.

Overall, catalytic data show that low-severity desilicated NaY zeolites could be better supports in combination with magnesium for the glucose isomerisation into fructose. They present improved activity and higher fructose productivity than the parent catalyst, and they can still be successfully regenerated. The potential of these catalysts is also higher than that of the previously reported higher magnesium content NaY zeolites.

Acknowledgement

This work was performed with financial support from EPSRC(UK) under grant EP/K014749/1. Solid-state NMR spectra were obtained at the EPSRC UK National Solid-state NMR Service at Durham.

Appendix A. Supplementary data

Supplementary data associated with this article can be found, in the online version, at http://dx.doi.org/10.1016/j.apcatb.2017.11.009.

References

[1] G.W. Huber, S. Iborra, A. Corma, Synthesis of transportation fuels from biomass: chemistry, catalysts, and engineering, Chem. Rev. 106 (2006) 4044–4098.
[2] V. Menon, M. Rao, Trends in bioconversion of lignocellulose: biofuels platform chemicals & biorefinery concept, Prog. Energy Combust. Sci. 38 (2012) 522–550.
[3] S.K. Maity, Opportunities, recent trends and challenges of integrated biorefinery: part I, Renew. Sustain. Energy Rev. 43 (2015) 1427–1445.
[4] S. Octave, D. Thomas, Biorefinery: toward an industrial metabolism, Biochimie 91 (2009) 659–664.
[5] M.J. Climent, A. Corma, S. Iborra, Converting carbohydrates to bulk chemicals and fine chemicals over heterogeneous catalysts, Green Chem. 13 (2011) 520–540.
[6] J. Song, H. Fan, J. Ma, B. Han, Conversion of glucose and cellulose into value-added products in water and ionic liquids, Green Chem. 15 (2013) 2619–2635.
[7] H. Li, P.S. Bhadury, A. Riisagerc, S. Yang, One-pot transformation of polysaccharides via multi-catalytic processes, Catal. Sci. Technol. 4 (2014) 4138–4168.
[8] M. Aresta, A. Dibenedetto, F. Dumeignil, Biorefinery Biomass to Chemicals and Fuels, De Gruyter, Germany, 2012.
[9] Bio-based Chemicals: Value Added Products from Biorefineries, IEA Bioenergy, 2012.
[10] J.N. Chheda, G.W. Huber, J.A. Dumesic, Liquid-phase catalytic processing of biomass-derived oxygenated hydrocarbons to fuels and chemicals, Angew. Chem. Int. Ed. 46 (2007) 7164–7183.
[11] X. Qian, Mechanisms and energetics for brønsted acid-catalyzed glucose condensation, dehydration and isomerization reactions, Top. Catal. 55 (2012) 218–226.
[12] R.-J. van Putten, J.C. van der Waal, E. de Jong, C.B. Rasrendra, H.J. Heeres, J.G. de Vries, Hydroxymethylfurfural, a versatile platform chemical made from renewable resources, Chem. Rev. 113 (2013) 1499–1597.
[13] I. Delidovich, R. Palkovits, Catalytic isomerization of biomass-derived aldoses: a review, ChemSusChem 9 (2016) 547–561.
[14] T. Buntara, S. Noel, P.H. Phua, I. Melián-Cabrera, J.G. de Vries, H.J. Heeres, Caprolactam from renewable resources: catalytic conversion of 5-hydroxymethylfurfural into caprolactone, Angew. Chem. Int. Ed. 50 (2011) 7083–7087.
[15] R. Beerthuis, G. Rothenberg, N.R. Shiju, Catalytic routes towards acrylic acid, adipic acid and ε-caprolactam starting from biorenewables, Green Chem. 17 (2015) 1341–1361.
[16] V.J. Jensen, S. Rugh, Industrial-scale production and application of immobilized glucose isomerase, Methods Enzymol. 136 (1987) 356–370.
[17] K. Buchholz, J. Seibel, Industrial carbohydrate biotransformations, Carbohydr. Res. 343 (2008) 1966–1979.
[18] C. Moreau, R. Durand, A. Roux, D. Tichit, Isomerization of glucose into fructose in the presence of cation-exchanged zeolites and hydrotalcites, Appl. Catal. A: Gen. 193 (2000) 257–264.
[19] J. Lecomte, A. Finiels, C. Moreau, Kinetic study of the isomerization of glucose into fructose in the presence of anion-modified hydrotalcites, Starch/Stärke 54 (2002) 75–79.
[20] C. Moreau, J. Lecomte, A. Roux, Determination of the basic strength of solid catalysts in water by means of a kinetic tracer, Catal. Commun. 7 (2006) 941–944.
[21] S. Yu, E. Kim, S. Park, I.K. Song, J.C. Jung, Isomerization of glucose into fructose over Mg–Al hydrotalcite catalysts, Catal. Commun. 29 (2012) 63–67.
[22] R. Shukla, X.E. Verykios, R. Mijtharasan, Isomerization and hydrolysis reactions of important disaccharides over inorganic heterogeneous catalysts, Carbohydr. Res. 143 (1985) 97–106.
[23] L. Lv, X. Guo, P. Bai, S. Zhao, Isomerization of glucose into fructose and mannose in presence of anion-exchanged resins, Asian J. Chem. 27 (2015) 2774–2778.
[24] R.O.L. Souza, D.P. Fabiano, C. Feche, F. Rataboul, D. Cardoso, N. Essayem, Glucose–fructose isomerisation promoted by basic hybrid catalysts, Catal. Today 195 (2012) 114–119.
[25] A.A. Marianou, C.M. Michailof, A. Pineda, E.F. Iliopoulou, K.S. Triantafyllidis, A.A. Lappas, Glucose to fructose isomerization in aqueous media over homogeneous and heterogeneous catalysts, ChemCatChem 8 (2016) 1100–1110.
[26] S. Lima, A.S. Dias, Z. Lin, P. Brandão, P. Ferreira, M. Pillinger, J. Rocha, V. Calvino-Casilda, A.A. Valente, Isomerization of D-glucose to D-fructose over metallosilicate solid bases, Appl. Catal. A: Gen. 339 (2008) 21–27.
[27] I. Graça, D. Iruretagoyena, D. Chadwick, Glucose isomerisation into fructose over magnesium-impregnated NaY zeolite catalysts, Appl. Catal. B: Environ. 206 (2017) 434–443.
[28] M. Moliner, Y. Román-Leshkov, M.E. Davis, Tin-containing zeolites are highly active catalysts for the isomerization of glucose in water, PNAS 107 (2010) 6164–6168.
[29] C.M. Lew, N. Rajabbeigi, M. Tsapatsis, Tin-containing zeolite for the isomerization of cellulosic sugars, Microporous Mesoporous Mater. 153 (2012) 55–58.
[30] G. Li, E.A. Pidko, E.J.M. Hensen, Synergy between Lewis acid sites and hydroxyl groups for the isomerization of glucose to fructose over Sn-containing zeolites: a theoretical perspective, Catal. Sci. Technol. 4 (2014) 2241–2250.
[31] J.C. Groen, J.A. Moulijn, J. Pérez-Ramirez, Desilication: on the controlled generation of mesoporosity in MFI zeolites, J. Mater. Chem. 16 (2006) 2121–2131.

[32] J.C. Groen, L.A.A. Peffer, J.A. Moulijn, J. Pérez-Ramirez, Mechanism of hierarchical porosity development in MFI zeolites by desilication: the role of aluminium as a pore-directing agent, Chem. Eur. J. 11 (2005) 4983–4994.
[33] J.C. Groen, W. Zhu, S. Brouwer, S.J. Huynink, F. Kapteijn, J.A. Moulijn, J. Pérez-Ramirez, Direct demonstration of enhanced diffusion in mesoporous ZSM-5 zeolite obtained via controlled desilication, J. Am. Chem. Soc. 129 (2007) 355–360.
[34] M. Ogura, S. Shinomiya, J. Tateno, Y. Nara, M. Nomura, E. Kikuchi, M. Matsukata, Alkali-treatment technique-new method for modification of structural and acid-catalytic properties of ZSM-5 zeolites, Appl. Catal. A: Gen. 219 (2001) 33–43.
[35] J.C. Groen, L.A.A. Peffer, J.A. Moulijn, J. Pérez-Ramirez, Mesoporosity development in ZSM-5 zeolite upon optimized desilication conditions in alkaline medium, Colloids Surf. A: Physicochem. Eng. Aspects 241 (2004) 53–58.
[36] L. Ren, Q. Guo, P. Kumar, M. Orazov, D. Xu, S.M. Alhassan, K.A. Mkhoyan, M.E. Davis, M. Tsapatsis, Self-pillared, single-unit-cell Sn-MFI zeolite nanosheets and their use for glucose and lactose isomerization, Angew. Chem. Int. Ed. 54 (2015) 10848–10851.
[37] P.Y. Dapsens, C. Mondelli, J. Jagielski, R. Hauert, J. Pérez-Ramírez, Hierarchical Sn-MFI zeolites prepared by facile top-down methods for sugar isomerisation, Catal. Sci. Technol. 4 (2014) 2302–2311.
[38] G. Yang, E.A. Pidko, E.J.M. Hensen, The mechanism of glucose isomerization to fructose over Sn-BEA zeolite: a periodic density functional theory study, ChemSusChem 6 (2013) 1688–1696.
[39] D. Verboekend, G. Vilé, J. Pérez-Ramírez, Hierarchical Y and USY zeolites designed by post-synthetic strategies, Adv. Funct. Mater. 22 (2012) 916–928.
[40] D. Verboekend, N. Nuttens, R. Locus, J. Van Aelst, P. Verolme, J.C. Groen, J. Pérez-Ramírez, B.F. Sels, Synthesis, characterisation, and catalytic evaluation of hierarchical faujasite zeolites: milestones, challenges, and future directions, Chem. Soc. Rev. 45 (2016) 3331–3352.
[41] P.A. Jacobs, W.J. Mortier, An attempt to rationalize stretching frequencies of lattice hydroxyl groups in hydrogen-zeolites, Zeolites 2 (1982) 226–230.
[42] V.L. Zholobenko, L.M. Kustov, V. Yu Borovkov, V.B. Kazansky, A new type of acidic hydroxyl groups in ZSM-5 zeolite and in mordenite according to diffuse reflectance i.r. spectroscopy, Zeolites 8 (1988) 175–178.
[43] I. Graça, A.M. Carmo, J.M. Lopes, M.F. Ribeiro, Improving HZSM-5 resistance to phenolic compounds for the bio-oils/FCC feedstocks co-processing, Fuel 140 (2015) 484–494.
[44] M. Hunger, J. Karger, H. Pfeifer, J. Caro, B. Zibrowius, M. Bulow, R. Mostowicz, Investigation of internal silanol groups as structural defects in ZSM-5-type zeolites, J. Chem. Soc. Faraday Trans. I 83 (1987) 3459–3468.
[45] A. Vimont, F. Thibault-Starzyk, J.C. Lavalley, Infrared spectroscopic study of the acidobasic properties of beta zeolite, J. Phys. Chem. B 104 (2000) 286–291.
[46] M. Jiangt, H.G. Karge, FTIR study of the kinetics of solid-state ion exchange in zeolites using pyridine as a probe, J. Chem. Soc. Faraday Trans. 91 (1995) 1845–1851.
[47] F. Maugé, A. Sahibed-Dine, M. Gaillard, M. Ziolek, Modification of the acidic properties of NaY zeolite by H2S, adsorption–an infrared study, J. Catal. 207 (2002) 353–360.
[48] M. Guisnet, P. Ayrault, J. Datka, Acid properties of dealuminated mordenites studied by IR spectroscopy. 2. Concentration, acid strength and heterogeneity of OH groups, Pol. J. Chem. 71 (1997) 1455–1461.
[49] W. Lutz, H. Toufar, D. Heidemann, N. Salman, C.H. Rüscher, T.M. Gesing, J.-Chr. Buhl, R. Bertram, Siliceous extra-framework species in dealuminated Y zeolites generated by steaming, Microporous Mesoporous Mater. 104 (2007) 171–178.
[50] W. Lutz, D. Heidemann, R. Kurzhals, G. Kryukova, Characterisation of siliceous extra-framework species in DAY zeolites by 29Si MAS NMR and IR spectroscopic measurements, Allg. Chem. 636 (2010) 1361–1367.
[51] W.Q. Jiao, W.H. Fu, X.M. Liang, Y.M. Wang, M.-Y. He, Preparation of hierarchically structured Y zeolitewith low Si/Al ratio and its applications in acetalization reactions, RSC Adv. 4 (2014) 58596–58607.
[52] M.A. Aramendía, J.A. Benítez, V. Borau, C. Jiménez, J.M. Marinas, J.R. Ruiz, F. Urbano, Characterization of various magnesium oxides by XRD and 1H MAS NMR spectroscopy, J. Solid State Chem. 144 (2009) 25–29.
[53] A.A. Rownaghi, R.L. Huhnke, Producing hydrogen-rich gases by steam reforming of syngas tar over CaO/MgO/NiO catalysts, ACS Sustain. Chem. Eng. 1 (2013) 80–86.
[54] N. Badar, N.F. Chayed, R. Rusdi, N. Kamarudin, N. Kamarulzaman, Band gap energies of magnesium oxide nanomaterials synthesized by the sol–gel method, Adv. Mater. Res. 545 (2012) 157–160.
[55] M. Fernández-Garcia, J.A. Rodriguez, Metal Oxide Nanoparticles, Chemistry Department, Brookhaven National Laboratory, 2007 BNL-79479-2007-BC.
[56] K.R. Nemade, S.A. Waghuley, Synthesis of MgO nanoparticles by solvent mixed spray pyrolysis technique for optical investigation, Int. J. Metals 2014 (2014) 1–4. Article ID 389416.
[57] N.F. Chayeda, N. Badara, R. Rusdia, N. Kamarudin, N. Kamarulzaman, Optical band gap energies of magnesium oxide (MgO) thin film and spherical nanostructures, AIP Conf. Proc. 1400 (2011) 328–332.
[58] L.A. Palacio, E.R. Silva, R. Catalão, J.M. Silva, D.A. Hoyos, F.R. Ribeiro, M.F. Ribeiro, Performance of supported catalysts based on a new copper vanadate-type precursor for catalytic oxidation of toluene, J. Hazard. Mater. 153 (2008) 628–634.
[59] Z. Liu, Z. Zhang, W. Xing, S. Komarneni, Z. Yan, X. Gao, X. Zhou, Tailoring acidity of HZSM-5 nanoparticles for methyl bromide dehydrobromination by Al and Mg incorporation, Nanoscale Res. Lett. 9 (2014) 550.
[60] X. Huang, Y. Men, J. Wang, W. An, Y. Wang, Highly active and selective binary MgO–SiO2 catalysts for the production of 1,3-butadiene from ethanol, Catal. Sci. Technol. 7 (2017) 168–180.
[61] F.X. Llabrés i Xamena, A. Zecchina, FTIR spectroscopy of carbon dioxide adsorbed on sodium- and magnesium-exchanged ETS-10 molecular sieves, Phys. Chem. Chem. Phys. 4 (2002) 1978–1982.
[62] J.I. Di Cosimo, V.K. Díez, C. Ferretti, C.R. Apesteguía, Basic catalysis on MgO: generation, characterization and catalytic properties of active sites, Catalysis 26 (2014) 1–28.
[63] C. Morterra, G. Ghiotti, F. Boccuzzi, S. Coluccia, An infrared spectroscopic investigation of the surface properties of magnesium aluminate spinel, J. Catal. 51 (1978) 299–313.
[64] M.W. Roberts, J.M. Thomas, Surface and Defect Properties of Solids vol. 2, The Chemical Society, London, 1973.
[65] T. Kanno, M. Kobayashi, Evaluation of basicity of alkali metal-doped MgO in the scope of change of carbonate species, Stud. Surf. Sci. Catal. 90 (1994) 207–212.
[66] Y. Ono, H. Hattori, Solid Base Catalysis, Springer, 2011.
[67] H.G. Karg, Infrared spectroscopic and catalytic studies on mordenite-like zeolites, ACS Symp. Ser. 40 (1977) 584–595.
[68] A. Penkova, L.F. Bobadilla, F. Romero-Sarria, M.A. Centeno, J.A. Odriozola, Pyridine adsorption on NiSn/MgO–Al2O3: an FTIR spectroscopic study of surface acidity, Appl. Surf. Sci. 317 (2014) 241–251.
[69] J.I. Di Cosimo, V.K. Díez, M. Xu, E. Iglesia, C.R. Apesteguía, Structure and surface and catalytic properties of Mg-Al basic oxides, J. Catal. 178 (1998) 499–510.
[70] T. Belin, C. Mve Mfoumou, S. Mignard, Y. Pouilloux, Study of physisorbed carbon dioxide on zeolites modified by addition of oxides or acetate impregnation, Microporous Mesoporous Mater. 182 (2013) 109–116.
[71] J.I. Di Cosimo, V.K. Díez, C. Ferretti, C.R. Apesteguía, Basic catalysis on MgO: generation, characterization and catalytic properties of active sites, Catalysis 26 (2014) 1–28.
[72] Y.B. Tewari, R.N. Goldberg, Thermodynamics of the conversion of aqueous glucose to fructose, J. Sol. Chem. 13 (1984) 523–547.
[73] I. Graça, M.C. Bacariza, D. Chadwick, Glucose isomerisation into fructose over Mg-impregnated Na-zeolites: influence of zeolite structure, Microporous Mesoporous Mater. 255 (2018) 130–139.
[74] Y. Ye, Q. Liu, J. Wang, Influence of saccharides chelating agent on particle size and magnetic properties of Co2Z hexaferrite synthesized by sol–gel method, J. Sol–Gel Sci. Technol. 60 (2011) 41–47.
[75] O. Fruhwirth, G.W. Herzog, I. Hollerer, A. Rachett, Dissolution and hydration kinetics of MgO, Surf. Technol. 24 (1985) 301–317.